ACS Sustainable Chemistry & Engineering

Research Article

pubs.acs.org/journal/ascecg

Role of Hydrochar Properties on the Porosity of Hydrochar-based Porous Carbon for Their Sustainable Application

Xiangdong Zhu, Yuchen Liu, Feng Qian, Chao Zhou, Shicheng Zhang,* and Jianmin Chen

Shanghai Key Laboratory of Atmospheric Particle Pollution and Prevention (LAP3), Department of Environmental Science and Engineering, Fudan University, Handan Road 220, Shanghai 200433, China

Supporting Information

ABSTRACT: In recent years, chemical activation of hydrochar (a solid material from hydrothermal carbonization (HTC) of lignocellulosic biomass) has been shown to be effective in producing advanced porous materials. However, the linkage between the properties of hydrochar and the porosity of hydrochar-based porous carbon (a material from the chemical activation of hydrochar) has not yet been clearly explored. In the present study, the results indicated that the properties of hydrochar (including stability, thermal recalcitrance, aromaticity and polarity) were greatly affected by the HTC process (peak temperature and retention time). Accordingly, the porosities of hydrochar-based porous carbon (including surface area and pore volume) were determined by the properties of hydrochar. For instance, positive correlations were founded between porosities of porous carbon materials and element compositions (H/C, O/C, and (O+N)/C) of hydrochar materials. Moreover, negative correlations were observed between the porosities of porous carbon materials and thermal recalcitrance of hydrochar materials. In general, a porous carbon with high porosity was produced from a hydrochar with HTC process of low peak temperature and retention time. Undoubtedly, hydrochar-based porous carbons retain features characteristic of its parent material.

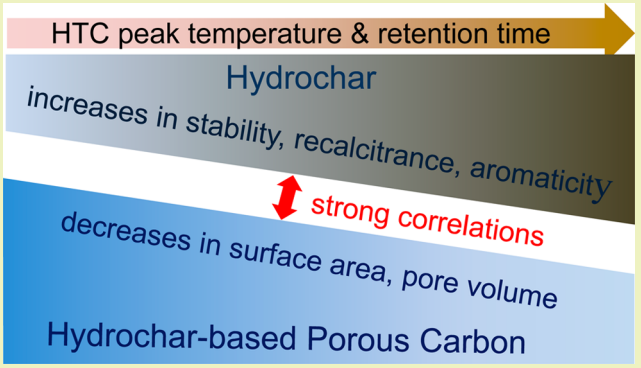

KEYWORDS: *Hydrochar, Properties, Porous carbon, Porosity, Correlation*

INTRODUCTION

Hydrothermal carbonization (HTC) has shown great potential over the past decade for conversion of biomass under mild processing temperatures owing to the simultaneous collection of bio-oil, high-value chemicals, and hydrochar material.[1−6] Hydrochar, a solid material from HTC process of biomass, exhibits lower H/C and O/C ratios than raw biomass owing to the development of H_2O and CO_2 through dehydration and decarboxylation reactions, resulting a high carbon content and a well-developed aromatic nature for hydrochar material.[7] And, hydrochar has lower ash content than conventional char owing to the separation of the soluble mineral constituent from the feedstock to the liquid phase, rendering it suitable as a template for fabrication of advanced porous material.[8−11] However, one of the main disadvantages hindering the effective and straightforward utilization of hydrochar material for final application is its low surface area and undeveloped porosity.[12−16] Consequently, postcarbonization methods are required to develop its porosity.

Very recently, the activation of hydrochar material by KOH, K_2CO_3, NaOH, and H_3PO_4 has been investigated, with the resultant porous carbon material (a material from the chemical activation of hydrochar, referred as hydrochar-based porous carbon) found to possess high surface area and narrow micropore size distributions.[17−20] Waste carbonaceous material activated by zinc chloride ($ZnCl_2$) can also produce porous carbon of high porosity.[21,22] However, few efforts have been focused on the activation of hydrochar by $ZnCl_2$. In addition, considerable progress has been achieved recently in understanding the effects of activation conditions (such as activation temperature, kind and quantity of activator) on the porosity of hydrochar-based porous carbon.[8,12,23,24] Research has found that the porosity of hydrochar-based porous carbon can be tailored through the modification of activation conditions, with the resultant porous carbon material exhibiting great potential for H_2 storage, CO_2 capture, and pollutant removal from aqueous solution.[8,13,23]

Furthermore, although increasing attention has recently been given to the activation of hydrochar derived from HTC process of homogeneous substrates (such as D-glucose, cellulose, furfural, starch, and saccharose), the activation of hydrochar from heterogeneous waste substrates (such as lignocellulosic biomass) remains less well understood.[12,19,23] The complexity of lignocellulosic biomass greatly influences resulting hydrochar

Received: December 15, 2014
Revised: March 27, 2015
Published: April 7, 2015

DOI: 10.1021/acssuschemeng.5b00153
ACS Sustainable Chem. Eng. 2015, 3, 833−840

properties through various HTC conditions. It is generally known that HTC process conditions (such as peak temperature and retention time) can be varied, leading to even wider variations in the chemical properties of hydrochar.[25] For example, decreases in O/C and H/C ratios occur with increasing HTC peak temperature and retention time.[26,27] As such, structural variations in hydrochar induced by different HTC processing conditions play an important role in the aromaticity, polarity, stability, and recalcitrance of the hydrochar itself.[1,25,28] Interestingly, Falco et al. recently reported that the temperature of the HTC process extensively affects porosity development in hydrochar-based porous carbon.[12] Furthermore, the porosity of hydrochar-based porous carbon can be modified by the properties of the hydrochar itself, and the porosity is tightly related to the performances of porous carbon.[29] However, to date, the linkage between the properties of hydrochar and the porosity of hydrochar-based porous carbon remains unknown.

The present study explores $ZnCl_2$ activation of hydrochar, with the main objective being to provide insights into the role of hydrochar properties in determining the porosity of hydrochar-based porous carbon. For this purpose, first, the effects of different HTC processing conditions (including peak temperature and retention time) on the properties of hydrochar materials (including thermogravimetry and elemental composition) were investigated. Then, $ZnCl_2$ was used to activate different hydrochar materials, with a thorough investigation for the porosity of hydrochar-based porous carbon (including surface area and pore volume). Finally, the correlation between the studied properties of hydrochar materials and the porosity of hydrochar-based porous carbon was built, in order to draw insights into the role of HTC conditions in determining the performance of hydrochar-based porous carbon. This study is noteworthy in that it represents a first attempt to investigate such correlations, with no such research to date in the literature.

EXPERIMENTAL SECTION

Synthesis of Hydrochar Materials. Hydrochar materials were prepared through HTC of *Salix psammophila* (SP), one of the dominant desert shrubs in Northern China. The raw SP were crushed and filtered through a 60-mesh sieve. The ash content of SP was determined as 10.72%, and the content of C, H, and O was determined to be 47.34%, 8.22%, and 33.33%, respectively. The cellulose, hemicellulose, and lignin contents were 55.5%, 18.9%, and 25.9%, respectively. HTC experimental conditions can be summarized as follows. A mixture of feedstock (15 g) and deionized water (150 mL) was added into an autoclave. The reactor was programmed to heat and then hold at a peak temperature with a set retention time. The reactor was run at an autogenic pressure of 0−8 MPa, measured by a pressure gauge. After reaction, the hydrochar products were washed several times with deionized water and dried overnight at 80 °C. To evaluate the effect of temperature, the SP feedstock was carbonized at five different peak temperatures (namely 180, 210, 240, 270, and 300 °C) for 1 h. To examine the effect of retention time, the SP feedstock was carbonized at four different hold times under peak temperature of 240 °C (namely 0, 0.5, 1, and 2 h), and peak temperature was selected as 240 °C to highlight the role of retention time. The each hydrochar were produced in duplicate. The prepared hydrochar materials were denoted using an $H-T-R$ labeling system, where H is hydrochar, T is HTC peak temperature (°C), and R is HTC retention time (h).

Chemical Activation of Hydrochar Materials. Hydrochar materials were chemically activated using zinc chloride ($ZnCl_2$). The solution of hydrochar material and activating reagent was mixed for 24 h under continuous agitation conditions (200 rpm) and then air-dried at 80 °C for 4 h. The weight ratio of $ZnCl_2$ to hydrochar material was 1:1.[15] Pretreated hydrochar was activated at 700 °C for 60 min under nitrogen (N_2) flow of 1 L/min at a heating rate of 4 °C/min. After the reactor was cooled to room temperature under N_2 flow, the carbonized sample was successively washed with 0.1 M hydrogen chloride (HCl), ethanol (wash the composition that undissolved in water), and water, before finally being dried in an oven at 100 °C for 4 h. Hydrochar-based porous carbon was denoted using a PC−T−R labeling system, where PC is porous carbon, T is HTC peak temperature (°C), and R is HTC retention time (h).

To further examine the effects of activator kind, the selected hydrochar materials were also activated using potassium carbonate (K_2CO_3) under the same activation conditions. However, in this case, the weight ratio of K_2CO_3 to hydrochar material was 1:2.[13]

Characterization of Hydrochar and Porous Carbon Materials. Nitrogen (N_2) adsorption isotherms of hydrochar-based porous carbon were determined at −196 °C using a conventional volumetric technique (Quantachrome, Quantasorb SI). Surface area was calculated using the Brunauer−Emmett−Teller (BET) method from adsorption data obtained in the relative pressure (p/p_0) range of 0.04−0.3. The total pore volume was determined from the amount of N_2 adsorbed at a p/p_0 value of 0.99. Micropore surface area and micropore volume were calculated via the t-plot analysis. Pore size distribution was evaluated via density functional theory (DFT) method using N_2 adsorption data.

CO_2 adsorption isotherms were also obtained at 0 °C using an ASAP 2020 volumetric adsorption analyzer (Micromeritics). The pore size distribution of the narrow microporosity region was also examined via the DFT method, using CO_2 adsorption data at 0 °C.

Elemental composition (C, H, N) was analyzed with an elemental analyzer (Vario EL III). The amount of ash in hydrochar materials was measured by air-heating the samples at 700 °C for 2 h. The functional groups of the hydrochar samples were examined using Fourier transform-infrared (FT-IR, Nexus 470) techniques. The morphology of samples was examined through scanning electron microscopy (SEM, S4800) and transmission electron microscopy (TEM, Tecnai G2). Thermogravimetry (TG) and derivative thermogravimetry (DTG) analysis of hydrochar samples were performed using a thermogravimetric analyzer (PerkinElmer), with heating conditions from 30−1000 °C under a N_2 atmosphere at a rate of 20 °C/min. The stability index (i.e., mass loss, in %) is calculated using the following equation:

$$\text{mass loss}(\%) = 100 - \text{residual mass}(\%)$$

where the residual mass is obtained directly from TG curves at a temperature of 700 °C (determined under a N_2 atmosphere).

To further calculate the thermal recalcitrance index (R_{50}), the hydrochar samples were also determined through TG technology under an air atmosphere. Harvey et al. developed an R_{50} index to quantitatively evaluate the recalcitrance of carbonaceous materials; this uses the energy required for thermal oxidation of carbonaceous materials as a measure of recalcitrance, and is calculated as follows[30,31]

$$R_{50} = \frac{T_{50,\text{hydrochar}}}{T_{50,\text{graphite}}}$$

where T_{50}, hydrochar, and T_{50}, graphite are the temperature values corresponding to 50% weight loss by oxidation and volatilization of hydrochar sample and graphite, respectively. The values of T_{50}, hydrochar, and T_{50}, graphite were obtained directly from TG thermograms (air atmosphere) corrected for water and ash content. The reference substance, graphite (purity 99.9995%, 100 mesh), was purchased from Alfa Aesar. A more detailed account for the calculation of R_{50} is given in previous literature by Harvey.[30]

RESULTS AND DISCUSSION

Thermogravimetric Analysis of Hydrochar Materials. TG investigations (under a N_2 atmosphere) revealed that mass

DOI: 10.1021/acssuschemeng.5b00153
ACS Sustainable Chem. Eng. 2015, 3, 833−840

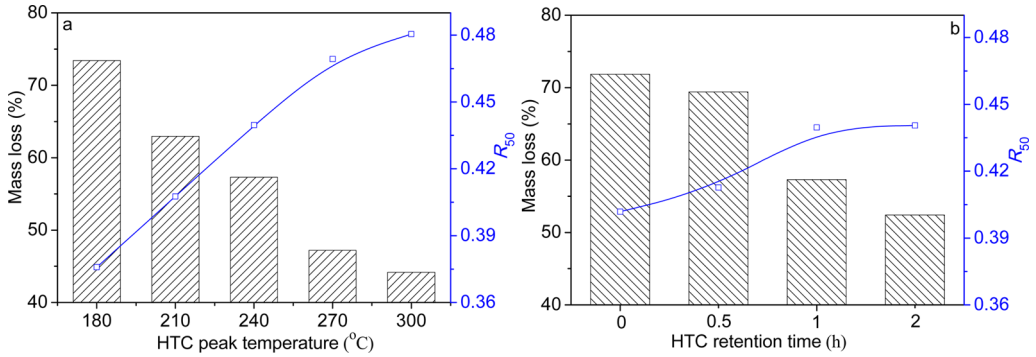

Figure 1. Mass loss (%) and R_{50} index of hydrochar sample as a function of (a) HTC peak temperature and (b) HTC retention time.

Table 1. Yields, Ash Contents, Elemental Compositions and Atomic Ratios of Different Hydrochar Materials

sample	yield (%)[a]	ash[b]	C (%)[c]	O (%)[c]	H (%)[c]	N (%)[c]	H/C[d]	O/C[e]	(O+N)/C[f]
H-180-1	64.72	8.57	55.29	35.61	8.65	0.45	1.88	0.48	0.49
H-210-1	58.49	8.17	57.62	33.51	8.30	0.58	1.73	0.44	0.44
H-240-1	49.02	8.26	64.11	26.90	8.42	0.58	1.58	0.31	0.32
H-270-1	39.75	8.20	72.54	18.48	8.15	0.83	1.35	0.19	0.20
H-300-1	35.02	7.92	73.58	17.71	7.90	0.80	1.29	0.18	0.19
H-240-0	55.84	6.36	54.30	36.85	8.28	0.57	1.83	0.51	0.52
H-240-0.5	51.79	7.12	58.18	33.41	7.80	0.61	1.61	0.43	0.44
H-240-2	43.26	7.44	65.31	26.09	7.76	0.84	1.43	0.30	0.31

[a]Yields are on a water-free basis. [b]Ash are on a water-free basis. [c]Elemental compositions are on a water- and ash-free basis. [d]H/C: atomic ratio of hydrogen to carbon. [e]O/C: atomic ratio of oxygen to carbon. [f](O+N)/C: atomic ratio of sum of oxygen and nitrogen to carbon.

loss of hydrochar materials decreased with progression of the HTC reaction, as shown in Figure 1, and the Supporting Information Figures S1 and S2. Hence, hydrochar materials became more stable with progression of the HTC reaction. This is because HTC reaction progressively reduces labile organic matter and produces more stable matter.

To further explain variations in thermal stability of hydrochar materials, differences in DTG curves were also considered. The DTG curves could be divided into four regions, and detailed explanations for the classification of region of DTG curves are given in the Supporting Information.[13,14,32] Hydrochar materials have been reported to possess a complex mixture of alkyl, aromatic, and carbohydrate moieties,[3,4,33] as indicated by the relative FT-IR spectra (shown in Figure S3 of the Supporting Infomation, detailed explanations for the FT-IR spectra are given in Supporting Information); these products could be degraded during the thermal process. As can be expected, the intensity of DTG peaks located within region II (resulted from thermo-oxidative degradation of susceptible products) decreased progressively with increasing HTC peak temperature, whereas DTG peaks located in region III (resulted from the loss of aromatic moisture) became more marked (Figure S1 of the Supporting Information). Accordingly, hydrochar materials produced at a higher HTC peak temperature should be more chemically stable. This is consistent with the weight loss results, obtained from TG curves. Similar results to those described here were obtained with variations in the retention time of the HTC process; however, the chemical stability of hydrochar materials appears to be influenced to a greater degree by peak temperature than by retention time, due to the fact that peak temperature induced a larger variation range in the ratio of mass loss.

To calculate quantitatively the recalcitrance ability of hydrochar materials, TG analysis was also conducted under an air atmosphere. As shown in Figure 1, the R_{50} index of hydrochar material increased gradually with increasing peak temperature and retention time, indicating that hydrochar materials produced at higher peak temperatures and with longer retention times would be more thermal recalcitrant. These findings are in agreement with results obtained from TG analysis conducted under a N_2 atmosphere, described earlier in this section.

Elemental Composition of Hydrochar Materials. Table 1 provides numerical results of elemental analysis of hydrochar materials, with yields and ash contents. As expected, yields declined gradually with increasing peak temperature and retention time owing to the increasing extent of liquefaction and gasification of raw SP feedstock.[34] However, ash content did not alter substantially across the various hydrochar materials.

As shown in Table 1, a gradual increase in C and N content, and a corresponding loss of H and O content occurred as peak temperature and retention time increased owing to intermolecular deoxygenation and dehydration reactions taking place during the HTC process.[27,33] Furthermore, molar ratios of elements are used to estimate aromaticity (H/C) and polarity (O/C, (O+N)/C).[25,35] It was observed that an increase in peak temperature produced a decrease in H/C and O/C atomic ratios (see Table 1), indicating an increase in the degree of condensation of hydrochar materials.[28] Hence, high aromaticity and low polarity (low H/C and O/C) were thus observed at higher peak temperatures.[35] A similar trend was noted with an increase in retention time.

The influence of HTC conditions on the degree of hydrochar condensation is a major factor driving thermal stability and recalcitrance, as indicated by the strong correlations between the molar ratios of H/C, O/C, and (O+N)/C and the characteristics of TG analysis (such as mass loss and R_{50})

DOI: 10.1021/acssuschemeng.5b00153
ACS Sustainable Chem. Eng. 2015, 3, 833−840

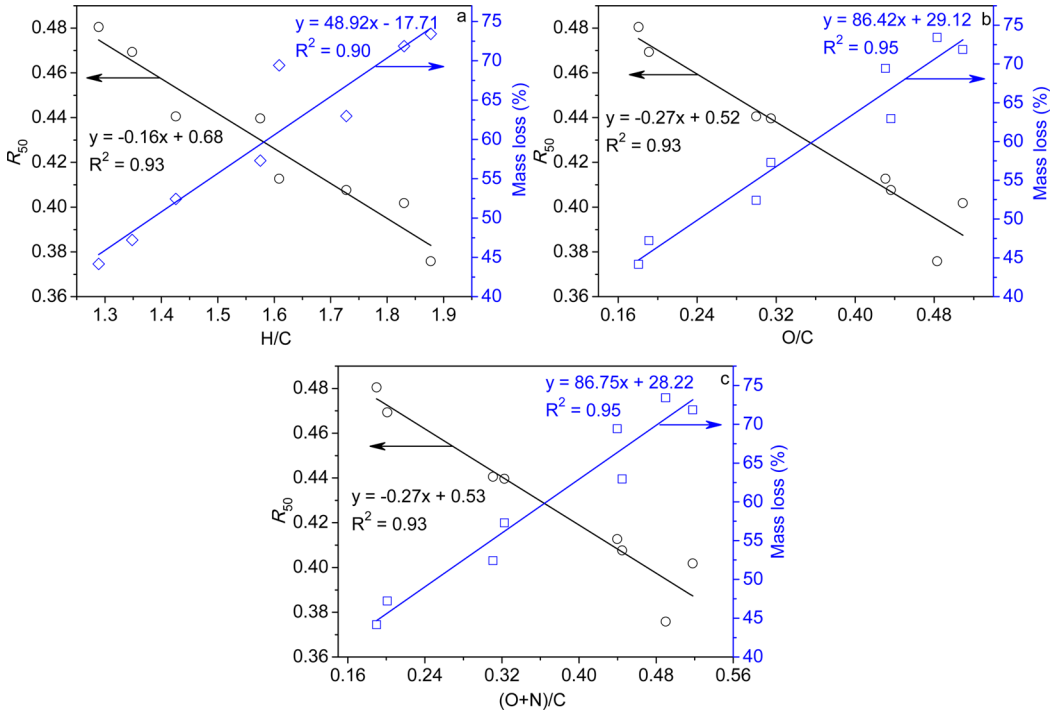

Figure 2. Correlations between TG characteristics of hydrochar (R_{50} values and mass loss (%)), and elemental composition characteristics of hydrochar (H/C, O/C, and (O+N)/C).

Table 2. Yields, Ash Contents, Elemental Compositions and Atomic Ratios of Different Hydrochar- based Porous Carbon Materials (Activator: $ZnCl_2$)

sample	yield (%)[a]	ash[b]	C (%)[c]	O (%)[c]	H (%)[c]	N (%)[c]	H/C[d]	O/C[e]	(O+N)/C[f]
PC-180-1	33.98	1.21	87.00	9.56	2.44	0.99	0.34	0.08	0.09
PC-210-1	35.23	2.69	85.53	11.10	2.21	1.17	0.31	0.10	0.11
PC-240-1	39.46	3.74	88.42	7.79	2.41	1.38	0.33	0.07	0.08
PC-270-1	43.23	7.22	86.85	9.29	2.33	1.53	0.32	0.08	0.10
PC-300-1	44.83	7.96	86.25	9.93	2.33	1.49	0.32	0.09	0.10
PC-240-0	35.90	1.76	86.49	9.88	2.41	1.21	0.34	0.09	0.10
PC-240-0.5	34.59	4.17	84.57	11.96	2.16	1.31	0.31	0.11	0.12
PC-240-2	40.61	5.13	83.90	12.33	2.33	1.45	0.33	0.11	0.12

[a]In g of porous carbon/100 g of hydrochar. [b]Ash are on a water-free basis. [c]Elemental compositions are on a water- and ash-free basis. [d]H/C: atomic ratio of hydrogen to carbon. [e]O/C: atomic ratio of oxygen to carbon. [f](O+N)/C: atomic ratio of sum of oxygen and nitrogen to carbon.

(Figure 2). The linkage between TG characteristics (such as mass loss and R_{50}) and the properties of hydrochar material (H/C) is further supported by the relevant FT-IR spectra. As shown in Figure S3 of the Supporting Information, condensation of hydrochar material increased with peak temperature and retention time, as indicated by a decrease in OH character (3416 cm^{-1}) and an increase in aromatic C═C character (1616 cm^{-1}). Overall, characteristics related to the elemental composition of hydrochar materials are in keeping with data obtained through TG characterization techniques.

Elemental and Morphological Analysis of Hydrochar-based Porous Carbon. The hydrochar were then activated to produce porous carbon. As shown in Table 2, the elemental composition (C, H, O, and N) of hydrochar-based porous carbon remained very similar, regardless of changes in HTC reaction conditions. Similar findings were reported in a previous work by Falco.[12] However, a porous carbon with relatively high yield was obviously derived from a hydrochar with high HTC peak temperature and retention time, suggesting that more stable hydrochar appears to resist chemical activation.

Morphological changes between hydrochar and porous carbon were investigated using SEM (Figure 3). SEM images of hydrochar material revealed the presence of microspheric particles resulting from transformation of the raw material and its subsequent precipitation and growth as spheres, with raw material retaining its cellular appearance.[8] Hydrochar material lacked porosity and had low surface area, with these mainly resulting from interparticle voids. However, after chemical activation with $ZnCl_2$, abundant micropores were produced (Figure 3c). This was further confirmed through the TEM image shown in Figure 3d.

Porous Textural Characteristics of Hydrochar-based Porous Carbon. As a Lewis acid, $ZnCl_2$ promote the reaction of aromatic condensation and emission of tar. This will result in the increases of the porous carbon porosity. The BET surface area of hydrochar-based porous carbon (activated without chemical activator) was only 300 m^2/g.[16] The nitrogen adsorption isotherms of different hydrochar-based porous

DOI: 10.1021/acssuschemeng.5b00153
ACS Sustainable Chem. Eng. 2015, 3, 833−840

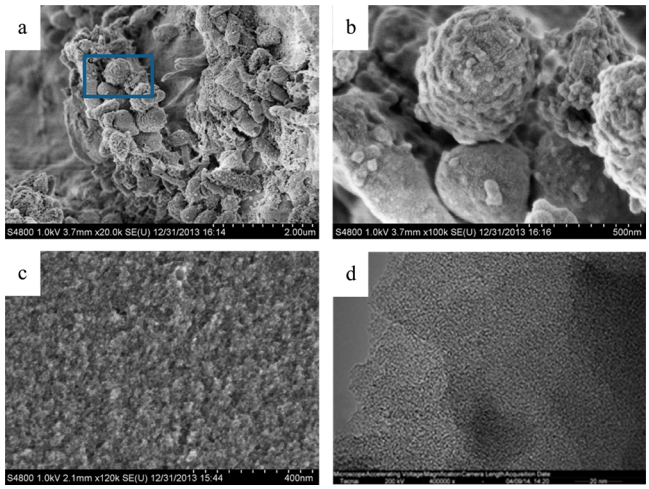

Figure 3. SEM images of (a) hydrochar produced at 300 °C and with 1 h HTC process retention time, (b) magnification of a specific region, (c) hydrochar-based porous carbon. Image d shows a TEM image of hydrochar-based porous carbon. In cases c and d, hydrochar was produced at 300 °C and with 1 h retention time.

carbon materials derived from $ZnCl_2$ activation are shown in Figure S4 of the Supporting Information, with the corresponding textural parameters summarized in Table 3, confirmed that $ZnCl_2$ is a good activator for the hydrochar activation.

As expected, all porous carbon materials exhibited a type I isotherm, typical of microporous materials. The N_2 adsorption isotherms of hydrochar-based porous carbon in Figure S4a of the Supporting Information show that there was a downward shift in N_2 adsorption when the production temperature of precursor materials (hydrochar) increased from 180 to 300 °C. Accordingly, the BET surface area and pore volume decreased with the production temperature of hydrochar. For instance, as the production temperature of hydrochar increased to 300 °C, the BET surface area and the micropore surface area decreased by 35.83% and 33.80%, respectively, while total pore volume and micropore volume decreased by 37.50% and 32.76%, respectively. However, the proportion of microporosity (indicated by V_{mic}/V_T) remained unchanged with changes in production temperature, except in the case of sample PC-180-1. Changes in the retention time of the HTC process produced similar results.

To further examine the effects of activator kind, the selected hydrochar materials were also activated using K_2CO_3. Obviously, hydrochar-based porous carbons derived from the K_2CO_3 activation had higher surface area and pore volume. However, hydrochar-based porous carbons derived from the $ZnCl_2$ activation had higher proportion of microsurface area and micropore volume. Interestingly, a similar trend to that described above was observed, with a higher BET surface area and pore volume obtained with lower production temperatures of hydrochar materials, as further confirmed by N_2 uptake isotherms (Figure S4c of the Supporting Information). Accordingly, as the production temperature of hydrochar increased to 300 °C, the BET surface area and the micropore surface area decreased by 33.92% and 29.71%, respectively, while total pore volume and micropore volume decreased by 35.11% and 30.16%, respectively (Table 3).

The pore size distribution (>0.7 nm) of the selected hydrochar-based porous carbon was studied through DFT methods using measured adsorption of N_2 at −196 °C.[20] Interestingly, the pore size distribution of porous carbon remained similar independently of the nature of hydrochar and of the type of activator used (Figure S5 of the Supporting Information). The analysis of pore size distribution suggests that porosity of porous carbon is mainly made up of micropores of approximately 1.1 and 1.6 nm, as indicated by the proportion of microporosity. In addition, a small amount of mesopores of up to approximately 5.2 nm was observed.

CO_2 adsorption isotherms of hydrochar-based porous carbon are presented in Figure S6 of the Supporting Information, with CO_2 uptake also shown in Table 3. The studied hydrochar-based porous carbon exhibited great potential for CO_2 adsorption. It is noteworthy that sample PC-300-1 had the lowest CO_2 uptake, with both $ZnCl_2$ and K_2CO_3 activation. This is due primarily to the fact that the volume of fine micropores in porous carbon is affected by the properties of the carbon precursor, as indicated by its relatively low surface area and pore volume. The pore size distribution of the microporosity region of porous carbon with $ZnCl_2$ activation had a similar shape, with micropores mainly distributed in the region of 0.45−0.60 and 0.8−0.9 nm (Figure S7 of the Supporting

Table 3. Textural Properties of Different Hydrochar-based Porous Carbon Materials

sample	S_{BET}[a] (m^2/g)	S_{mic}[b] (m^2/g)	S_{mic}/S_{BET} (%)	V_{mic}[c] (cm^3/g)	V_t[d] (cm^3/g)	V_{mic}/V_t (%)	n_{CO2}[e] (mmol/g)
activator: $ZnCl_2$							
PC-180-1	1308	1187	90.75	0.58	0.72	80.56	3.97
PC-210-1	1178	1105	93.80	0.55	0.63	87.30	3.85
PC-240-1	1096	1007	91.88	0.50	0.59	84.75	3.95
PC-270-1	947.1	883.7	93.31	0.44	0.51	86.27	3.49
PC-300-1	839.3	785.8	93.63	0.39	0.45	86.67	3.05
PC-240-0	1296	1192	91.98	0.59	0.70	84.29	4.07
PC-240-0.5	1180	1081	91.61	0.53	0.64	82.81	3.98
PC-240-2	1030	943.7	91.62	0.47	0.56	83.93	4.00
activator: K_2CO_3							
PC-180-1	1459	1261	86.43	0.63	0.94	67.02	5.91
PC-240-1	1244	1133	91.08	0.57	0.77	74.03	5.93
PC-300-1	964.1	886.3	91.93	0.44	0.61	72.13	4.93

[a]Measured using N_2 adsorption with the Brunauer−Emmett−Teller (BET) method. [b]Micropore surface area calculated using *t*-plot method. [c]Micropore volume calculated using the *t*-plot method. [d]Total pore volume determined at $P/P_0 = 0.99$. [e]n_{CO2} is CO_2 adsorption capacity at 0 °C and 0.03 bar.

DOI: 10.1021/acssuschemeng.5b00153
ACS Sustainable Chem. Eng. 2015, 3, 833−840

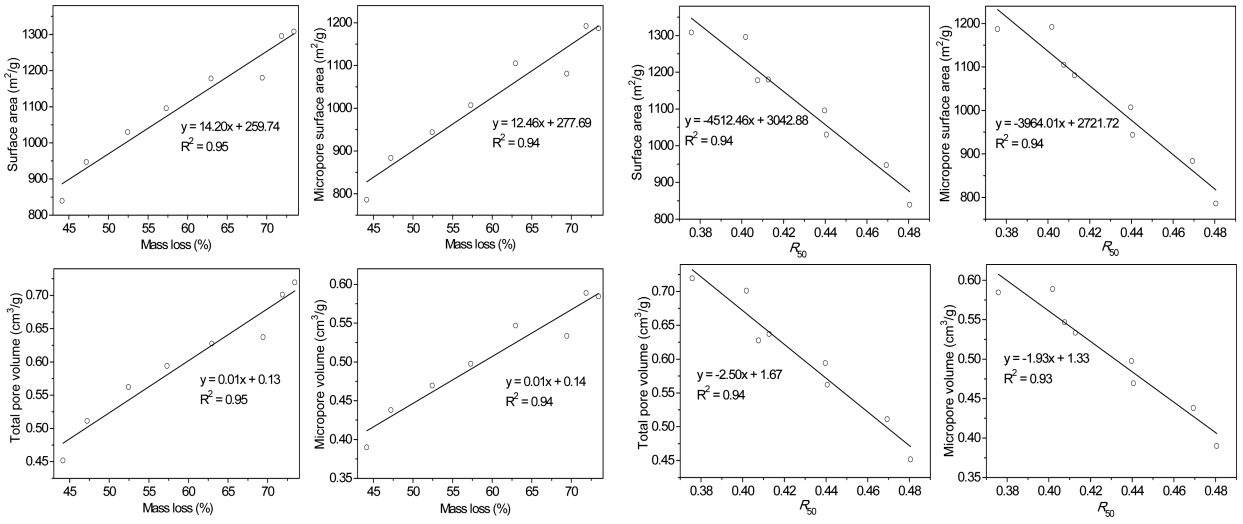

Figure 4. Correlations between the porosity of hydrochar-based porous carbon (activator: $ZnCl_2$) and TG characteristics of hydrochar.

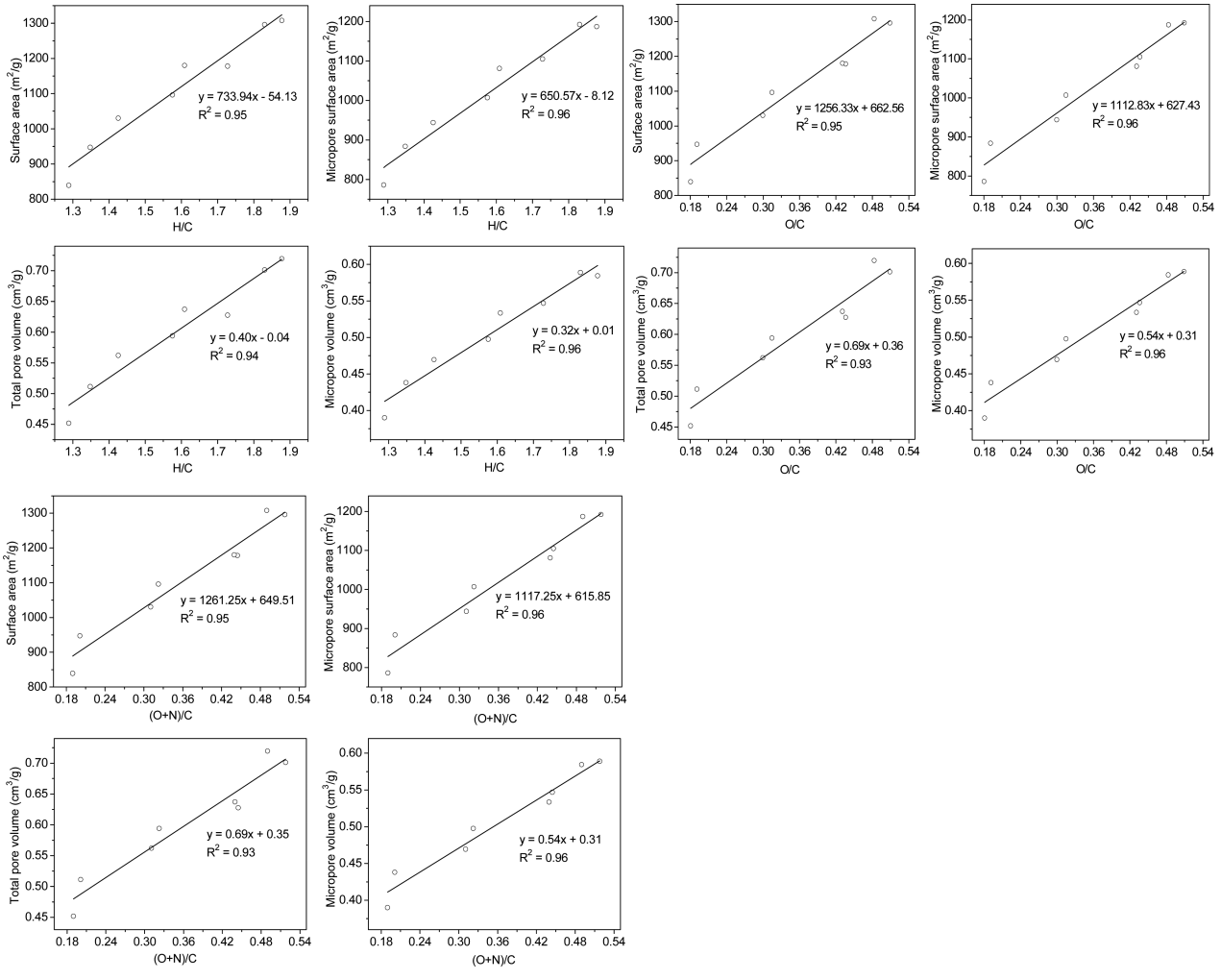

Figure 5. Correlations between porosity of hydrochar-based porous carbon (activator: $ZnCl_2$) and elemental composition characteristics of hydrochar (H/C, O/C, and (O+N)/C atomic ratio).

Information). However, K_2CO_3-porous carbon exhibited a broader microporosity distribution, as confirmed by its relatively high CO_2 adsorption capacity.

Overall, this result shows that the conditions of the HTC process strongly affect the porosity of hydrochar-based porous carbon. Generally, hydrochar produced at a lower peak temperature and with lesser retention time generates porous carbon with higher porosity. Furthermore, hydrochar-based porous carbon retains memory of the properties of its parent material.

DOI: 10.1021/acssuschemeng.5b00153
ACS Sustainable Chem. Eng. 2015, 3, 833−840

Correlations between Hydrochar Properties and Porosity of Porous Carbon. It has been well documented in the literature that the porosity of hydrochar-based porous carbon is determined by a combination of the properties of its carbon precursor and activation conditions.[8,12,19,20,23] However, to develop the porosity of resultant products, more attention should be paid to the optimization of activation process. Here, to gain a direct comparison of the porosity of different porous carbons, the characteristics of TG and elemental composition of hydrochar materials (such as mass loss, R_{50} index, and H/C, O/C, and (O+N)/C atomic ratios) were plotted against the porosity of porous carbon materials, taking into account surface area, micropore surface area, total pore volume, and micropore volume (Figures 4 and 5, and Figures S8−12 of the Supporting Information). Thus, under a given set of activation conditions, the properties of hydrochar material could be used to determine the porosity of porous carbon.

As previously noted, hydrochar materials became more stable and recalcitrant with progression of the HTC reaction. As shown in Figures 4 and 5, a linear increase in porosity was obtained as a function of the mass loss, while a linear decrease in porosity occurred as a function of the R_{50} index, indicating that the development of porosity in hydrochar-based porous carbon is greatly affected by the properties of hydrochar. It is evident that the development of porosity of hydrochar-based porous carbon is inhibited with progression of the HTC reaction and is determined by the stability and recalcitrance of its precursor. Correspondingly, high porosity in hydrochar-based porous carbon is observed from hydrochar with HTC process of low production temperature and retention time. To gain further insights into the performance of porous carbon, the porosities of the hydrochar-based porous carbon were further correlated with the elemental composition of hydrochar materials, as shown in Figures S6−8 of the Supporting Information. Positive correlations ($R^2 \geq 0.93$) were observed between the porosities of hydrochar-based porous carbon and the atomic ratio of hydrochar materials (H/C, O/C, and (O+N)/C), suggesting that the porosity of hydrochar-based porous carbon is also determined by the aromaticity (H/C) and polarity (O/C, (O+N)/C) of its precursor. Correspondingly, porous carbon with high porosity was observed from a carbon precursor with low aromaticity and high polarity. These trends can be explained by taking into account the dependence of the chemical structure of hydrochar on production conditions.[12] As per previous literature and our results, an increase in peak temperature and retention time in the HTC process appears to lead to an increase in aromatization and a reduction in polarity functional groups of hydrochar.[9] More aromatized structure and lower polar functional groups in a hydrochar material may thus inhibit the development of porosity of its porous carbon product, due to the formation of more stable and recalcitrant carbon precursors as a result of resisting cross-linking reactions (cyclization and condensation processes) during the chemical activation process.

To examine the effects of the activator, the porosity of selected hydrochar-based porous carbon materials, activated with K_2CO_3, was also correlated with the characteristics of TG and elemental compositions of carbon precursors, as shown in Figures S8−12 of the Supporting Information. As expected, hydrochar of low recalcitrance produced a material with high porosity. Similar correlations were thus observed, regardless of the kind of activator used.

CONCLUSIONS

In this work, the relationship between the properties of hydrochar and the porosity of hydrochar-based porous carbon material was studied in detail. An increase in peak temperature and retention time of the HTC process led to increased stability, thermal recalcitrance, and aromaticity of hydrochar materials, together with a decrease in polarity characteristics. Furthermore, HTC conditions were found to have an extensive effect on the development of porosity in hydrochar-based porous carbon. Further, positive correlations were observed between porosities (surface area, micropore surface area, total pore volume, and micropore volume) of porous carbon materials and properties of hydrochar materials (including mass loss, H/C, O/C, and (O+N)/C). Moreover, negative correlations were observed between the porosities of porous carbon materials and recalcitrance (R_{50} index) of hydrochar materials. In general, hydrochar derived from the HTC process of low peak temperature and retention time will produce porous carbon with high porosity. This study provided new insight into the HTC conditions on the performance of hydrochar-based porous carbon, which was an important procedure toward advanced porous carbon material. Undoubtedly, the feedstock type also affects the hydrochar property, and its role on the porosity of hydrochar-based porous carbon needs to be explained in the future research.

ASSOCIATED CONTENT

Supporting Information

Additional information as noted in text. This material is available free of charge via the Internet at http://pubs.acs.org.

AUTHOR INFORMATION

Corresponding Author

*S. Zhang. Tel/fax: +86-21-65642297. E-mail: zhangsc@fudan.edu.cn.

Notes

The authors declare no competing financial interest.

ACKNOWLEDGMENTS

This research was supported by the National Natural Science Foundation of China (No. 21407027), National Key Technology Support Program (No. 2015BAD15B06), and Shanghai Talent Development Fund (No. 201414).

REFERENCES

(1) Xu, Q.; Qian, Q.; Quek, A.; Ai, N.; Zeng, G.; Wang, J. Hydrothermal carbonization of macroalgae and the effects of experimental parameters on the properties of hydrochars. *ACS Sustainable Chem. Eng.* **2013**, *1*, 1092−1101.

(2) Pham, M.; Schideman, L.; Scott, J.; Rajagopalan, N.; Plewa, M. J. Chemical and biological characterization of wastewater generated from hydrothermal liquefaction of *Spirulina*. *Environ. Sci. Technol.* **2013**, *47*, 2131−2138.

(3) Zhou, D.; Zhang, L.; Zhang, S.; Fu, H.; Chen, J. Hydrothermal liquefaction of macroalgae *Enteromorpha prolifera* to bio-oil. *Energy Fuels* **2010**, *24*, 4054−4061.

(4) Zhou, D.; Zhang, S.; Fu, H.; Chen, J. Liquefaction of macroalgae *Enteromorpha prolifera* in sub-/supercritical alcohols: direct production of ester compounds. *Energy Fuels* **2012**, *26*, 2342−2351.

(5) Changjun, L.; Xiao, Y.; Zhe, Z.; Dong, Z.; Liang, Z.; Shicheng, Z.; Jianmin, C. Hydrothermal liquefaction of desert shrub *Salix psammophila* to high value-added chemicals and hydrochar with recycled processing water. *BioResources* **2013**, *8*, 2981−2997.

DOI: 10.1021/acssuschemeng.5b00153
ACS Sustainable Chem. Eng. 2015, 3, 833−840

(6) Bargmann, I.; Martens, R.; Rillig, M. C.; Kruse, A.; Kücke, M. Hydrochar amendment promotes microbial immobilization of mineral nitrogen. *J. Plant Nutr. Soil Sci.* **2014**, *177*, 59−67.
(7) Libra, J. A.; Ro, K. S.; Kammann, C.; Funke, A.; Berge, N. D.; Neubauer, Y.; Titirici, M.-M.; Fühner, C.; Bens, O.; Kern, J. Hydrothermal carbonization of biomass residuals: A comparative review of the chemistry, processes and applications of wet and dry pyrolysis. *Biofuels* **2011**, *2*, 71−106.
(8) Sevilla, M.; Fuertes, A.; Mokaya, R. High density hydrogen storage in superactivated carbons from hydrothermally carbonized renewable organic materials. *Energy Environ. Sci.* **2011**, *4*, 1400−1410.
(9) Titirici, M.-M.; White, R. J.; Falco, C.; Sevilla, M. Black perspectives for a green future: Hydrothermal carbons for environment protection and energy storage. *Energy Environ. Sci.* **2012**, *5*, 6796−6822.
(10) Zhang, M.; Gao, B.; Fang, J.; Creamer, A. E.; Ullman, J. L. Self-assembly of needle-like layered double hydroxide (LDH) nanocrystals on hydrochar: Characterization and phosphate removal ability. *RSC Adv.* **2014**, *4*, 28171−28175.
(11) Dai, L.; Wu, B.; Tan, F.; He, M.; Wang, W.; Qin, H.; Tang, X.; Zhu, Q.; Pan, K.; Hu, Q. Engineered hydrochar composites for phosphorus removal/recovery: Lanthanum doped hydrochar prepared by hydrothermal carbonization of lanthanum pretreated rice straw. *Bioresour. Technol.* **2014**, *161*, 327−332.
(12) Falco, C.; Marco-Lozar, J.; Salinas-Torres, D.; Morallón, E.; Cazorla-Amorós, D.; Titirici, M.; Lozano-Castello, D. Tailoring the porosity of chemically activated hydrothermal carbons: Influence of the precursor and hydrothermal carbonization temperature. *Carbon* **2013**, *62*, 346−355.
(13) Zhu, X.; Liu, Y.; Zhou, C.; Zhang, S.; Chen, J. Novel and high-performance magnetic carbon composite prepared from waste hydrochar for dye removal. *ACS Sustainable Chem. Eng.* **2014**, *2*, 969−977.
(14) Zhu, X.; Liu, Y.; Qian, F.; Zhou, C.; Zhang, S.; Chen, J. Preparation of magnetic porous carbon from waste hydrochar by simultaneous activation and magnetization for tetracycline removal. *Bioresour. Technol.* **2014**, *154*, 209−214.
(15) Zhu, X.; Liu, Y.; Luo, G.; Qian, F.; Zhang, S.; Chen, J. Facile fabrication of magnetic carbon composites from hydrochar via simultaneous activation and magnetization for triclosan adsorption. *Environ. Sci. Technol.* **2014**, *48*, 5840−5848.
(16) Zhu, X.; Liu, Y.; Zhou, C.; Luo, G.; Zhang, S.; Chen, J. A novel porous carbon derived from hydrothermal carbon for efficient adsorption of tetracycline. *Carbon* **2014**, *77*, 627−636.
(17) Hao, W.; Bjorkman, E.; Lilliestråle, M.; Hedin, N. Activated carbons for water treatment prepared by phosphoric acid activation of hydrothermally treated beer waste. *Ind. Eng. Chem. Res.* **2014**, *53*, 15389−15397.
(18) Hao, W.; Björkman, E.; Yun, Y.; Lilliestråle, M.; Hedin, N. Iron oxide nanoparticles embedded in activated carbons prepared from hydrothermally treated waste biomass. *ChemSusChem* **2014**, *7*, 875−882.
(19) Romero-Anaya, A.; Ouzzine, M.; Lillo-Ródenas, M.; Linares-Solano, A. Spherical carbons: Synthesis, characterization and activation processes. *Carbon* **2014**, *68*, 296−307.
(20) Hao, W.; Björkman, E.; Lilliestråle, M.; Hedin, N. Activated carbons prepared from hydrothermally carbonized waste biomass used as adsorbents for CO_2. *Appl. Energy* **2013**, *112*, 526−532.
(21) Wang, T.; Tan, S.; Liang, C. Preparation and characterization of activated carbon from wood via microwave-induced $ZnCl_2$ activation. *Carbon* **2009**, *47*, 1880−1883.
(22) Juan, Y.; Ke-Qiang, Q. Preparation of activated carbon by chemical activation under vacuum. *Environ. Sci. Technol.* **2009**, *43*, 3385−3390.
(23) Sevilla, M.; Fuertes, A. B. Sustainable porous carbons with a superior performance for CO_2 capture. *Energy Environ. Sci.* **2011**, *4*, 1765−1771.
(24) Sevilla, M.; Falco, C.; Titirici, M.-M.; Fuertes, A. B. High-performance CO_2 sorbents from algae. *RSC Adv.* **2012**, *2*, 12792−12797.
(25) Cao, X.; Ro, K. S.; Libra, J. A.; Kammann, C. I.; Lima, I.; Berge, N.; Li, L.; Li, Y.; Chen, N.; Yang, J. Effects of biomass types and carbonization conditions on the chemical characteristics of hydrochars. *J. Agric. Food Chem.* **2013**, *61*, 9401−9411.
(26) Fuertes, A.; Arbestain, M. C.; Sevilla, M.; Maciá-Agulló, J.; Fiol, S.; López, R.; Smernik, R. J.; Aitkenhead, W.; Arce, F.; Macias, F. Chemical and structural properties of carbonaceous products obtained by pyrolysis and hydrothermal carbonisation of corn stover. *Soil Res.* **2010**, *48*, 618−626.
(27) Gao, Y.; Wang, X.; Wang, J.; Li, X.; Cheng, J.; Yang, H.; Chen, H. Effect of residence time on chemical and structural properties of hydrochar obtained by hydrothermal carbonization of water hyacinth. *Energy* **2013**, *58*, 376−383.
(28) Sevilla, M.; Fuertes, A. B. The production of carbon materials by hydrothermal carbonization of cellulose. *Carbon* **2009**, *47*, 2281−2289.
(29) Sevilla, M.; Mokaya, R. Energy storage applications of activated carbons: Supercapacitors and hydrogen storage. *Energy Environ. Sci.* **2014**, *7*, 1250−1280.
(30) Harvey, O. R.; Kuo, L.-J.; Zimmerman, A. R.; Louchouarn, P.; Amonette, J. E.; Herbert, B. E. An index-based approach to assessing recalcitrance and soil carbon sequestration potential of engineered black carbons (biochars). *Environ. Sci. Technol.* **2012**, *46*, 1415−1421.
(31) Zhao, L.; Cao, X.; Mašek, O.; Zimmerman, A. Heterogeneity of biochar properties as a function of feedstock sources and production temperatures. *J. Hazard. Mater.* **2013**, *256*, 1−9.
(32) Cimò, G.; Kucerik, J.; Berns, A. E.; Schaumann, G. E.; Alonzo, G.; Conte, P. Effect of heating time and temperature on the chemical characteristics of biochar from poultry manure. *J. Agric. Food Chem.* **2014**, *62*, 1912−1918.
(33) Kang, S.; Li, X.; Fan, J.; Chang, J. Characterization of hydrochars produced by hydrothermal carbonization of lignin, cellulose, D-xylose, and wood meal. *Ind. Eng. Chem. Res.* **2012**, *51*, 9023−9031.
(34) Falco, C.; Baccile, N.; Titirici, M.-M. Morphological and structural differences between glucose, cellulose and lignocellulosic biomass derived hydrothermal carbons. *Green Chem.* **2011**, *13*, 3273−3281.
(35) Ahmad, M.; Lee, S. S.; Dou, X.; Mohan, D.; Sung, J.-K.; Yang, J. E.; Ok, Y. S. Effects of pyrolysis temperature on soybean stover-and peanut shell-derived biochar properties and TCE adsorption in water. *Bioresour. Technol.* **2012**, *118*, 536−544.

DOI: 10.1021/acssuschemeng.5b00153
ACS Sustainable Chem. Eng. 2015, 3, 833−840